Electrodynamics of Highly Spin-Polarized Tunnel Josephson Junctions

H.G. Ahmad,[1,2,*] R. Caruso,[1,2,3] A. Pal,[4,5] G. Rotoli,[6] G.P. Pepe,[1,2] M.G. Blamire,[4] F. Tafuri,[1,2] and D. Massarotti[2,7]

[1]*Dipartimento di Fisica E. Pancini, Università degli Studi di Napoli Federico II, Monte S. Angelo, via Cinthia, Napoli, I-80126, Italy*

[2]*CNR-SPIN, c/o Complesso Monte Sant'Angelo, via Cinthia, I-80126, Napoli, Italy*

[3]*SeeQC-eu, via dei Due Macelli 66, Roma I-00187, Italy*

[4]*Department of Materials Science and Metallurgy, University of Cambridge, 27 Charles Babbage Road, Cambridge CB3 0FS, United Kingdom*

[5]*Department of Metallurgical Engineering and Materials Science, IIT Bombay, Mumbai 400076, India*

[6]*Dipartimento di Ingegneria, Università della Campania "Luigi Vanvitelli," via Roma 29, Aversa (CE) 81031, Italy*

[7]*Dipartimento di Ingegneria Elettrica e delle Tecnologie dell'Informazione, Università degli Studi di Napoli Federico II, via Claudio, Napoli, I-80125, Italy*

The continuous development of superconducting electronics is encouraging several studies on hybrid Josephson junctions (JJs) based on superconductor-ferromagnet-superconductor (SFS) heterostructures, as either spintronic devices or switchable elements in quantum and classical circuits. Recent experimental evidence of macroscopic quantum tunneling and of an incomplete 0-π transition in tunnel-ferromagnetic spin-filter JJs could also enhance the capabilities of SFS JJs as active elements. Here, we provide a self-consistent electrodynamic characterization of NbN/GdN/NbN spin-filter JJs as a function of the barrier thickness, disentangling the high-frequency dissipation effects due to the environment from the intrinsic low-frequency dissipation processes. The fitting of the I-V characteristics at 4.2 K and at 300 mK by using the tunnel-junction-microscopic model allows us to determine the subgap resistance R_{sg}, the quality factor Q, and the junction capacitance C. These results provide the scaling behavior of the electrodynamic parameters as a function of the barrier thickness, which represents a fundamental step for the feasibility of tunnel-ferromagnetic JJs as active elements in quantum and classical circuits, and are of general interest for tunnel junctions other than conventional SIS JJs.

I. INTRODUCTION

Ferromagnetic Josephson junctions (SFS JJs) have attracted considerable attention in the emerging fields of superconducting spintronics [1–5] and as quantum and classical devices, since they have been proposed as energy-efficient memories [6–9] and as passive π shifters (phase inverters) in quantum circuits [10–12]. However, in standard metallic SFS JJs, the I_cR_N product is of the order of a few microvolts or less [2,3,11], I_c and R_N being, respectively, the critical current and the normal state resistance. All these JJs are overdamped and thus characterized by high quasiparticle dissipation [11,13,14]. This has hampered the use of ferromagnetic JJs as active switching elements in different classical and quantum circuits, since for such applications it is important to have a rather high I_cR_N product and low damping [13]. Low-dissipative ferromagnetic junctions use an additional insulating layer between one of the superconducting electrodes and the ferromagnetic barrier (SIFS JJs) [7,15–17] or a ferromagnetic insulator barrier (SI$_f$ S JJs) [18–22] and may present key advantages for some applications, thus increasing the overall impact of JJs based on ferromagnetic barriers [7,16,17,23,24].

Heterostructures incorporating ferromagnetic insulator tunnel barriers have been theoretically proposed as quantum devices such as *quiet* ferromagnetic flux-qubits, based on anomalous 0-π transitions [19–21], and as classical devices for digital electronics [18] and efficient electron refrigeration [25]. Among the ferromagnetic insulators, GdN has been used in superconducting spin valves [26], switchable JJs based on the interfacial exchange field [27], and in spin-filter NbN/GdN/NbN JJs, which represent the first SI$_f$ S JJs. Some of their properties have been studied in

*halimagiovanna.ahmad@unina.it

Refs. [28–32]. The first evidence of macroscopic quantum tunneling (MQT) in ferromagnetic JJs is an indication that spin-filter JJs can be used as active quantum devices [31]. These JJs are characterized by a thickness-dependent spin polarization because of the splitting in the GdN insulator band structure induced by its magnetic exchange energy [28]. This property, together with the nontrivial magnetic structure of the barrier, causes an incomplete 0-π transition for the spin-filter efficiency (P) above 90%. Such an incomplete 0-π transition could be related to the presence of spin-triplet correlations, with implications for the 0-π technology [32].

This work aims at providing a self-consistent determination of the electrodynamic parameters in highly spin-polarized NbN/GdN/NbN junctions [Fig. 1 (a)]. For conventional JJs in the underdamped regime and with large I_c, measurements of Fiske steps have been successfully used to derive the capacitance C, while the amplitude of

(a) Nb top contact
SiO₂
SiO₂
SiO₂
NbN
MgO buffer layer
GdN I$_f$ barrier
NbN bottom contact
SiO₂ substrate

(b) Superconducting state
ω_p, Q_1
$\omega \sim 0, Q_0$
Voltage state
Current
Voltage

FIG. 1.   (a) A sketch showing spin-filter JJs. The area of the devices is 7×7 μm^2 (dashed blue window). Superconducting electrodes are NbN, while GdN is the ferromagnetic insulator (I_f) barrier. (b) The washboard potential of a Josephson junction. The brown double arrow represents the oscillating motion at the plasma frequency of the phase particle in the superconducting state. In this regime, the damping is determined by the high-frequency quality factor Q_1. The dashed green line represents the steady motion of the particle that rolls down the washboard in the voltage state. In this regime, the damping is determined by the low-frequency quality factor Q_0.

the hysteresis in the I-V curve allows us to estimate the quality factor Q within the resistively and capacitively shunted junction (RCSJ) model [33–35]. However, when the junctions fall in the moderately damped regime or are characterized by low values of I_c (or critical current density $J_c = I_c/A$, where A is the cross section), it is more complicated to isolate the effective capacitance and the intrinsic dissipation sources of the junction from contributions due to the environment and the external circuit. Thus, more sophisticated methods are required for the analysis of the dissipation [33,36–39]. We use the conventional tunnel-junction-microscopic (TJM) model to obtain a self-consistent estimation of C, Q, and the resistance associated with the quasiparticle dynamics R_{sg}, which are essential to define the electrodynamic properties of devices with I_c down to few nanoamperes. The merit of this approach is a comparative analysis of tunnel-ferromagnetic JJs with barrier thickness spanning from 2.5 to 4.0 nm. This allows us to explore substantially quite different transport regimes. If one wants to place the junction in a circuit or to couple it to a cavity [40,41], knowledge of the electrodynamic parameters and how they scale with the barrier thickness is fundamental. Therefore, this study provides a pathway to the engineering of tunnel-ferromagnetic JJs for specific applications.

II. METHODS

Dissipation in a JJ is frequency dependent and the quality factor is given by $Q(\omega) = \omega_p R(\omega) C$, where $\omega_p = (2eI_c/(\hbar C))^{1/2}$ is the plasma frequency [33–35]. In terms of the phase dynamics in the tilted washboard potential [33], the phase particle in the supercurrent branch oscillates in one well of the potential at the plasma frequency ω_p, while the voltage state involves steady motion of the phase particle ($\omega \sim 0$) [39] [Fig. 1(b)]. High-frequency (approximately ω_p) dissipation at the switching from the superconducting to the resistive state [see the brown double arrow in Fig. 1(b)] is determined by the high-frequency damping Q_1 and is mainly affected by the environment, i.e., the circuit in which the junction is embedded [36–39]. Low-frequency dissipation in the subgap branch of the I-V curves ($\omega \sim 0$) [see the green dashed arrow in Fig. 1(b)] and the corresponding low-frequency damping Q_0 are affected by the intrinsic tunnel resistance, which is set by the subgap resistance R_{sg} [38,39,42–44] as

$$Q_0 = \omega_p C R_{sg}. \qquad (1)$$

The TJM model provides a complete microscopic description of a JJ, using the tunneling-Hamiltonian formalism [33,34], and it is commonly employed for modeling superconducting quantum-interference devices (SQUIDs) and rapid-single-flux-quantum (RSFQ) logic gates and circuits [45–48]. This model can describe the subgap branch and the low-frequency electrodynamics of any JJ that shows
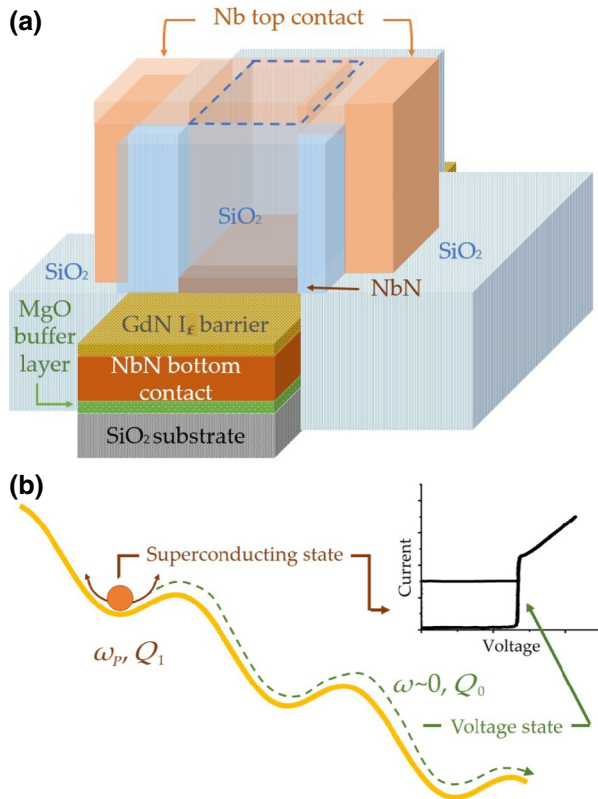
tunneling conduction, without taking into account the exact expression for the current-phase relation (CPR), which could be nontrivial in the case of unconventional JJs such as the spin-filter JJs analyzed in this work [30]. Therefore, it provides a powerful tool to investigate and determine Q_0 in junctions far from the underdamped regime and it enables us to isolate the dissipative components coming from the environment. It is particularly relevant since quasiparticle tunneling is a figure of merit in all classical and quantum circuits and has been, in general, a limit for standard SFS JJs. Measurements down to 300 mK of the I-V characteristics are performed by using an evaporation cryostat, while measurements down to 20 mK are performed in a wet dilution refrigerator. Customized RC, copper-powder filters, and room-temperature electromagnetic interference (EMI) filters guarantee high precision and resolution in the microvolt and nanoampere ranges. More details on the measurement setup can be found in Refs. [31,49], while information regarding the fabrication processes is given in Refs. [28,30,50]. We measure the I-V curves of junctions with different GdN thickness t at 20 mK, 300 mK, and 4.2 K by current biasing the samples with a triangular waveform at 11.123 Hz and by measuring the voltage across the junction. We extract I_c at a voltage value far from the noise detected in the supercurrent branch. The normal resistance R_N is calculated with a linear fit above $V_g = (\Delta_1 + \Delta_2)/e = 3.50$ mV, with Δ_1 and Δ_2 being the gap energies of the two superconducting NbN electrodes.

TJM simulations are calculated by using the PSCAN2 software [51], a PYTHON module optimized to simulate SFQ logic-based superconducting circuits that typically work at 4.2 K. One of the subroutines of this software allows to simulate the I-V characteristic of a JJ in electronic circuits with different degrees of complexity (the PSCAN2 subroutine calculates time-averaged voltages V across the device as a function of a bias current I). I_c, the Stewart-McCumber parameter $\beta = Q_0^2$, the gap voltage V_g, the ratio I_cR_N/V_g, and the ratio R_N/R_{sg}, R_{sg} being the resistance of the subgap branch, are the software parameters that govern the shape of the I-V curves. I_c and V_g, measured directly from the I-V curves in our experimental setup, are affected by errors of 1% and 2%, respectively, while R_N is obtained by fitting the ohmic region of the I-V curves and is affected by an error of 3%. Since these values can be obtained with high precision, they can be set as fixed parameters, as well as the ratio I_cR_N/V_g. β and the ratio R_N/R_{sg} are the fitting parameters. The Stewart-McCumber parameter modifies the amplitude of the hysteresis in the I-V curve, without affecting the subgap region [Fig. 2(a)]. The ratio R_N/R_{sg}, instead, modifies both the subgap shape and the hysteresis amplitude [Fig. 2(b)].

In our simulations, we reproduce the current biasing of a JJ with a current generator in series with the filtered lines of our experimental setup (approximately 200 Ω). For each
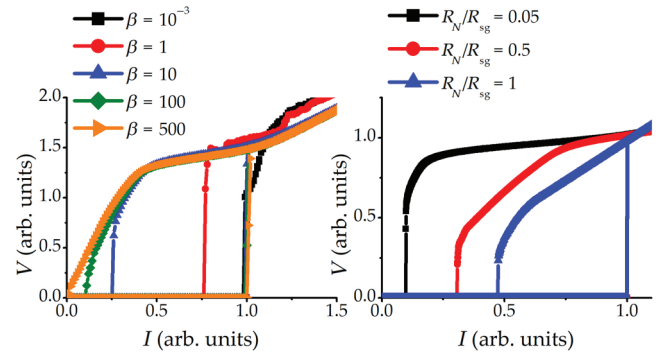

FIG. 2. I-V curves in normalized units simulated by using PSCAN2, by fixing $V_g = 1.4$, $I_cR_N = 1.0$: in (a), we fix $R_N/R_{sg} = 0.1$ and change β; while in (b), we fix $\beta = 10$ and change R_N/R_{sg}.

spin-filter JJ with a certain GdN thickness t, we choose the best-fit parameters Q_0 and R_{sg} in such a way that the deviations from the experimental curves are minimal. The errors on Q_0 and R_{sg} represent the range of values that provide a significant overlap between the experimental I-V characteristics and the simulated curves within the TJM model and are of 6% and 10%, respectively.

The GdN thicknesses in the junctions analyzed in this work range from 2.5 to 4.0 nm, while P ranges from 88% to 98%, respectively (Table II), falling in the highly spin-polarized regime. In the special case of spin-polarized systems, R_N has to be redefined as the combination of the two resistances associated with the presence of different tunnel conductances for spin-up and spin-down electrons, because of the spin-filtering effect (see the Appendix). The subgap shape in the I-V curves is linked to the quasiparticle dynamics in the junction. The quasiparticle current in a spin-polarized system has been expressed theoretically and analytically in the case of symmetric spin-filter JJs by taking into account the magnetic nature of the tunnel barrier and the spin-filtering effect [52]. Simple calculations allow us to verify that the quasiparticle current in these devices has the same expression both in the case of conventional tunnel JJs, i.e., for $P = 0$ and a magnetic exchange field in the tunnel barrier $h = 0$, and in the ideal and extreme situation of perfect spin polarization ($P = 100\%$) (see the Appendix). The conventional TJM model does not take into account the magnetic exchange field of the I_f barrier in spin-filter junctions, which can be important in the intermediate regime between these two extreme cases.

The systematic fitting of the I-V curves at 4.2 K as a function of the barrier thickness confirms that the shape of the I-V curves is mostly determined by the standard parameters of the junction (C, R_{sg}, Q_0). Further consistency is given by the I-V fitting through the frequency-dependent RCSJ model for the junction with the highest P, as shown in Sec. III. Below 4.2 K, NbN/GdN/NbN JJs with P up to 98% show an incipient 0-π transition in the
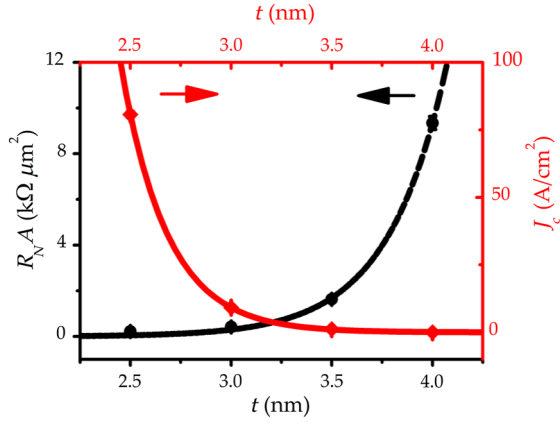
FIG. 3. In black, the $R_N A(t)$ product measured at 300 mK (black circles) as a function of the barrier thickness along with a fit using Eq. (2) (dashed curve). In red, the critical current density $J_c(t)$ measured at 300 mK as a function of the GdN thickness t (diamonds) along with an exponential fit (full line). The error bars are of the order of 1% on measured values for I_c and of 3% for R_N.

$I_c(T)$ curves, which can be understood in terms of spin-triplet correlations arising because of the presence of both the spin-filtering effect and nonuniform magnetic activity in the I_f barrier [32]. Therefore, deviations between the experimental curves and simulations at 300 mK can be due to the magnetic nature of the barrier, which the TJM model does not take into account. However, the estimated fitting parameters give an upper bound to Q_0 and R_{sg}, and a term of comparison for possible applications of spin-filter JJs at very low temperatures, as discussed in Sec. IV.

III. RESULTS

As one can observe in Fig. 3, the critical current density $J_c(t)$, with cross section $A = 49 \ \mu m^2$, and the $R_N A(t)$ curves at 300 mK obey typical tunnel behavior, thus confirming the insulating nature of the ballistic GdN barrier [32]. $R_N A(t)$ exhibits the characteristic exponential thickness dependence:

$$R_N A(t) = \frac{2tA}{3\sqrt{4m_e \bar{E}}} (h/e)^2 \, e^{(2t/\hbar)\sqrt{4m_e \bar{E}}}, \tag{2}$$

where m_e is the free electron mass, e is the electron charge, and $\bar{E}$ is the mean energy-barrier height seen by the charge

carriers [53]. In Table I, we report $I_c R_N$ at 4.2 K, at 300 mK, and at 20 mK, measured from the I-V curves. The characteristic voltage $I_c R_N$ decreases by increasing the barrier thickness, as well as the corresponding Josephson frequency $\omega_c = I_c R_N 2e/\hbar$. At 4.2 K, it ranges from 80 GHz for the thinnest junction to 1 GHz for the thickest one. At lower temperatures, we measure higher values of the $I_c R_N$ product. These values are higher than those usually achieved for SFS JJs and comparable to those of some SIFS heterostructures [1,3,7,11,15,16]. For barrier thicknesses lower than 2.5 nm, the characteristic voltage is as high as a few millivolts [28,31,32].

In Fig. 4, we present the I-V curves measured at 4.2 K (black points) and the TJM simulations (red straight lines) obtained by using PSCAN2. We collect in Table II the fitting parameters R_{sg} and Q_0. The thicker the barrier is, the higher is the subgap resistance [42–44]. The low-frequency quality factor Q_0 decreases with the thickness. This is due to both the decrease of I_c and of C of the barrier with the thickness [33].

The decrease in the Q_0 factor for increasing t indicates a smooth transition from an underdamped regime ($Q_0 \sim 10$) to a moderately damped regime with phase diffusion (PD) ($Q_0 \sim 1$) [39,54,55]. The presence of the PD regime is confirmed by the finite slope in the supercurrent branch for the junction with a 4.0-nm-thick barrier [39], which the PSCAN2 simulations cannot reproduce, since they do not take PD processes into account. Monte Carlo simulations can reproduce the finite slope in the supercurrent branch, taking into account multiple escape and retrapping processes in the phase dynamics, which are particularly relevant for low values of the Q_1 factor and the Josephson energy $E_J = \hbar I_c/2e$ comparable with the thermal energy $k_B T$, as in the case of the spin-filter junction with a 4.0-nm-thick barrier [39]. In Fig. 4(d), a Monte Carlo fit according to the frequency-dependent RCSJ model is shown (blue square points), with high-frequency $Q_1 = 0.13$ and low-frequency $Q_0 = 2.8$. This is consistent with the outcomes based on the TJM model.

The environment plays an important role in determining the value of Q_1. The ratio between the low- and high-frequency quality factors Q_1/Q_0 equals the ratio between the resistance of the environment R_{env} and the subgap resistance, R_{env}/R_{sg}, since Q_0 is written in terms

TABLE I. The parameters of the measured spin-filter junctions: the thickness t, the spin-filtering efficiency (P), and the characteristic voltage $I_c R_N$ at 4.2 K, 300 mK, and 20 mK. The errors on the characteristic voltage are given by a propagation of maximum errors on I_c (1%) and R_N (3%).

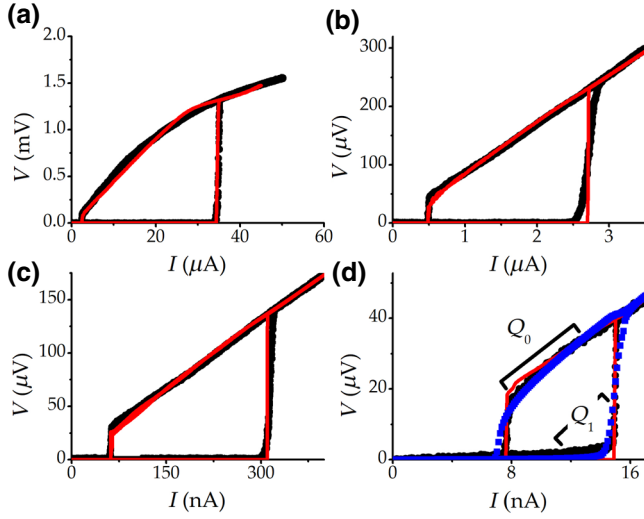| t (nm)	P (%)	$I_c R_N$ at 4.2 K (μV)	$I_c R_N$ at 300 mK (μV)	$I_c R_N$ at 20 mK (μV)
2.5	88	156 ± 3	179 ± 4	. . .
3.0	93	24.2 ± 0.5	38.3 ± 0.8	44.0 ± 0.9
3.5	96	9.9 ± 0.2	19.0 ± 0.4	. . .
4.0	98	2.8 ± 0.1	5.1 ± 0.2	6.1 ± 0.2

FIG. 4. The measured I-V curves at 4.2 K (black points) and TJM model simulation by using the PSCAN2 software (red curve) for high spin-filter JJs with thicknesses t of (a) 2.5, (b) 3.0, (c) 3.5, and (d) 4.0 nm. The quality factor Q_0 and subgap resistance R_{sg} estimated from the simulations are collected in Table II. The blue squares in (d) represent the frequency-dependent RCSJ model fit curve, obtained for $Q_0 = 2.8$ and $Q_1 = 0.13$.

of the quasiparticle dissipation [Eq. (1)], while Q_1 can be expressed in terms of the environment resistance R_{env} [37–39]. For the junction with a GdN barrier thickness of 4.0 nm, R_{env} is approximately 150 Ω, which is of the same order of magnitude of the resistance of the lines in our experimental setup.

Our analysis allows us to estimate the capacitance C of the barrier and its dependence on the barrier thickness, using Eq. (1) (see Table II). The value of C for the thinnest GdN barrier is consistent with a previous estimation based on measurements of switching current distribution (SCD) [31]. In Fig. 5, we plot the junction capacitance C as a function of the GdN barrier thickness t (black circle points) and the fitting function for the capacitance in a parallel-plate capacitor $C = \epsilon_0 \epsilon_r A/t$ (black dashed line), where $\epsilon_0 = 8.85$ pF/m is the vacuum dielectric permittivity and ϵ_r is the GdN relative permittivity, which acts as a fitting parameter. The estimated $\epsilon_r = (20 \pm 8)$ is consistent
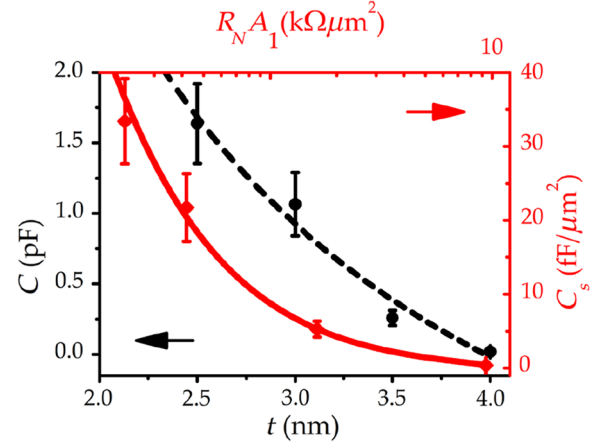

FIG. 5. In black: the capacitance values of spin-filter JJs as a function of the GdN barrier thickness t (black circles), along with parallel-plate capacitance $C(t)$ fit (dashed curve). In red: the specific capacitance C_s of the analyzed junctions as a function of $R_N A$ (red diamonds) along with a tunnel-barrier model fit [straight line; see Eq. (3)]. The error bars on C and C_s are calculated using the propagation of the errors on R_{sg}, Q_0, and I_c.

with the GdN permittivity $\epsilon_r = 26.5$ obtained with spectroscopic measurements on isolated GdN thin films [56], providing an additional validation of the fitting procedure. The $R_N A$ product as a function of the specific capacitance $C_s = C/A$ (red diamonds in Fig. 5), follows the expected behavior for tunnel JJs [57]. The red line in Fig. 5 is the function

$$R_N A(C_s) = \frac{2A\epsilon_0\epsilon_r}{3C_s\sqrt{4m_e\bar{E}}} (h/e)^2 e^{(2\epsilon_0\epsilon_r/\hbar C_s)\sqrt{4m_e\bar{E}}}, \quad (3)$$

which is obtained by replacing t in Eq. (2) with its dependence on the specific capacitance C_s, $t = \epsilon_0\epsilon_r/C_s$.

In Fig. 6(a), we show the I-V characteristic measured at 300 mK (black points) and TJM simulations (red straight lines) for the junction with a 4.0-nm-thick barrier, which corresponds to the highest spin-filtering efficiency analyzed in this work. Q_0 and R_{sg} for all the devices are collected in Table II. The best-fit curve at 300 mK is

TABLE II. The parameters of the measured spin-filter junctions: the thickness t, the subgap resistance R_{sg}, the quality factor Q_0, and the capacitance C, calculated using Eq. (1). R_{sg} and Q_0 are determined by fitting the I-V curves according to the TJM model. The errors on the subgap resistance and the quality factor are of the order of 10% and 6%, respectively, while the error on the capacitance (20%) is obtained by propagation of the errors on Q_0 and R_{sg}, and are of the same order of magnitude as those in Ref. [37].

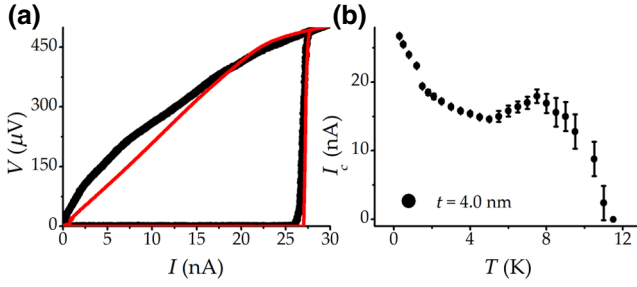| t (nm)	R_{sg} at 4.2 K (Ω)	R_{sg} at 300 mK (Ω)	Q_0 at 4.2 K	Q_0 at 300 mK	C (pF)
2.5	59	93	16	48	1.6
3.0	82	350	7.3	35	1.1
3.5	440	1700	6.6	32	0.26
4.0	3000	13 000	2.6	26	0.018

FIG. 6. (a) The measured I-V characteristic at 300 mK (black points) and the TJM model simulation by using the PSCAN2 software (red straight line) for the spin-filter JJ with $t = 4.0$ nm. The quality factor Q_0 and subgap resistance R_{sg} estimated from the simulations are collected in Table II. (b) The incipient 0-π transition in the $I_c(T)$ for the spin-filter JJ with $t = 4.0$ nm, as reported in Ref. [32].

FIG. 7. Normalized I-V curves at 20 mK (black points), 300 mK (red squares), and 4.2 K (blue diamonds) for spin-filter JJs with thicknesses t of (a) 3.0 nm and (b) 4.0 nm. The current is normalized to the critical current I_c, while the voltage is normalized to the switching value V_s.

characterized by a smaller R_{sg} compared to the experimental one. We can attribute this deviation to the unconventional magnetic activity discussed in Ref. [32], which is at a maximum in the case of most spin-polarized JJs, where the magnetic nature of the barriers manifests in a steep increase of $I_c(T)$ below 2 K [Fig. 6(b)] [32]. The conventional TJM model does not take the magnetic activity in the I_f barrier into account, nor the spin-dependent tunneling mechanism and the unconventional thermal behavior of I_c, thus giving a systematic underestimation of R_{sg}, as shown in Fig. 6(a). However, despite the presence of these deviations, R_{sg} estimated for all the junctions increases when decreasing the temperature T due to the tunnel nature of the conduction mechanisms in the system [43] and Q_0 increases because of the increase of R_{sg}, as expected.

In Fig. 7, we finally present a comparison between the normalized I-V curves measured at 4.2 K and 300 mK and the I-V characteristics at 20 mK for two of the junctions with the highest P: (a) $t = 3.0$ nm and $P = 93\%$ and (b) $t = 4.0$ nm and $P = 98\%$. The current is normalized to I_c, while the voltage is normalized to the switching value V_s to compare the subgap branches of the I-V curves. The I_c values at 20 mK are 4.75 μA for (a) and 29 nA for (b). The critical current at 300 mK is 4.64 μA for (a) and 26.7 nA for (b). The amplitude of the hysteresis in the I-V curves increases when going toward lower temperatures, pointing to an increase of Q_0 and also as a consequence of R_{sg}.

IV. DISCUSSION AND CONCLUDING REMARKS

The use of the TJM model on parent compounds allows us to achieve a consistent and robust picture of tunnel-ferromagnetic JJs with a quantitative insight on key electrodynamic parameters, such as Q_0, R_{sg}, and C.

The estimated Q_0 values at 4.2 K are up to 2 orders of magnitude higher compared to those of standard SFS heterostructures that typically operate in the overdamped
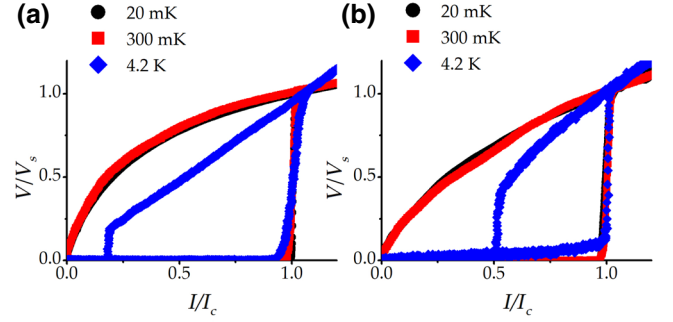
regime, such as SNS JJs, with β ranging from 10^{-3} to 10^{-1} [33,34,58]. The Q_0 values are of the same order of magnitude as those of conventional SIS junctions commonly used to drive components in quantum and classical circuits and for their readout [59,60]. Moreover, the Q_0 values increase up to one order of magnitude for the 4.0-nm-thick barrier, when lowering T to 300 mK. This sets a lower limit that can only increase at lower temperatures (see Fig. 7), and suggests possible implementation of spin-filter JJs in low-dissipative π-qubits. π-superconducting rf SQUIDS with ferromagnetic-insulating barriers have only been theoretically suggested as *quiet* qubits, efficiently decoupled from the fluctuations of an external magnetic field [20,21]. A spin-filter JJ with $t = 3.0$ nm and an $A \sim 50$ μm^2 has an estimated charging energy $E_c = e^2/(2C) \sim 900 \mu$K and a Josephson energy at 20 mK $E_J \sim 100$ K, which means that $E_J/E_c \sim 10^5$, suitable for a flux qubit [40,41].

In the frame of the 0-π technology, the spin-filter JJs analyzed in this work can also be implemented as complementary π junctions for the phase bias of a conventional flux qubit (passive elements) in which the high values of the subgap resistance R_{sg} could increase the dephasing time of the overall circuit [13]. The dephasing time is proportional to $E_J^2 R_{sg}$ of the π junction [13]. The subgap resistance in this work ranges from tens of ohms to some kilo-ohms at 4.2 K, but when T decreases, R_{sg} increases from a factor of 2 to 5. The dephasing time of a circuit with a spin-filter JJ with a $t = 3.0$ nm–thick barrier can be comparable with that of circuits with SIFS π junctions [15] and can increase by at least a factor of 100 compared to circuits with standard metallic π shifters [12,60]. In standard metallic SFS JJs, typical resistances are at most approximately 1 Ω, while R_{sg} for the junction with a 3.0-nm-thick barrier at dilution temperature is at least 350 Ω.

The subgap resistance is crucial for the engineering of transmon qubits. As suggested in Ref. [61], in these circuits quasiparticle tunneling can affect the relaxation

and coherence times [61]. The values obtained in this work can be promising even for potential application of tunnel-ferromagnetic JJs in transmon qubits. The order of magnitude of the ratio E_J/E_c for the investigated junctions scales with the thickness from 10^6 to 10. Adapting the area of the devices to conventional dimensions in transmon qubits ($A \sim 1\ \mu\text{m}^2$), lower values of E_J/E_c can be achieved, falling in the typical range of the transmon qubit [40,41,62]. As an example, by reducing the cross section to $A \sim 1\ \mu\text{m}^2$, E_J of the spin-filter JJ with $t = 3.5$ nm becomes approximately 280 mK, while E_c becomes approximately 180 mK, so that $E_J/E_c \sim 2$. Moreover, in reducing the junction area by a factor of approximately 50, R_{sg} should increase up to values of the order of 50–100 kΩ, thus further reducing quasiparticle noise. The same arguments are valid for the junction with a $t = 4.0$ nm GdN barrier, which is characterized by a subgap resistance that is approximately 10 times higher.

In conclusion, this work represents the first electrodynamic characterization of spin-filter JJs and a fundamental step to use these devices as active elements in superconducting circuits. Our comparative and self-consistent approach allows us to obtain the scaling law as a function of the barrier thickness of fundamental electrodynamic parameters, such as $C_s(t)$, $R_{\text{sg}}(t)$, and $Q_0(t)$, providing the possibility of engineering spin-filter JJs as a function of the junction area in order to meet specific circuit requirements. Even if the ferromagnetic JJs analyzed in this work are not ideal SIS JJs, we succeed in the determination of these fundamental electrodynamic parameters at 4.2 K by using a conventional TJM model and we provide a lower bound for R_{sg} and Q_0 at 300 mK. The underestimation of $R_{\text{sg}}(t)$ observed at 300 mK is due to the absence of the spin-filtering effect and of the magnetic activity of the barrier in the TJM model. Further studies are needed to implement a microscopic modelization of the peculiar properties of the I_f barrier, such as spin-selective tunneling mechanisms and triplet correlations.

The same approach can be successfully extended to different types of tunnel junctions other than conventional SIS JJs—for instance, multilayered SIFS JJs—and can provide the possibility of engineering special circuits other than conventional flux and transmon qubits, in which ferromagnetic tunnel junctions can be tuned by external microwaves and are capacitively coupled to standard superconducting circuits [23,24].

APPENDIX: THE SPIN-FILTERING EFFECT

Josephson junctions with GdN barriers show a spin-filtering effect due to the simultaneous presence of tunnel conduction mechanisms and a magnetic exchange field h in the ferromagnetic phase of the barrier. When the GdN becomes ferromagnetic ($T_{\text{Curie}} \sim 40$ K), the presence of exchange interactions leads to a spin selectivity of the tunneling processes: spin up (down) will see different barrier heights $E_{\uparrow(\downarrow)} = E_0 \mp h/2$, where E_0 is the energy-barrier height in the paramagnetic phase of the GdN. Carriers that experience a higher barrier will be filtered out, thus giving a net spin-polarized current [28].

An experimental measure of the spin-filtering efficiency is obtained from the $R(T)$ curves, since it can be defined as

$$P = \left| \frac{\sigma_\uparrow - \sigma_\downarrow}{\sigma_\uparrow + \sigma_\downarrow} \right|, \tag{A1}$$

where $\sigma_{\uparrow(\downarrow)}$ is the tunnel conductance through the barriers seen by spin up (down) carriers. In the limit of small magnetic exchange fields, the spin-filtering efficiency reduces to

$$P \sim \tanh \left[\coth^{-1} \left(\frac{R^*}{R} \right) \right], \tag{A2}$$

where R and R^* correspond to the measured resistance and the resistance in the absence of a magnetic exchange field, respectively [28].

In Fig. 8, we show the $R(T)$ curve (black points) for the spin-filter JJ with a GdN barrier thickness of 4.0 nm. The red straight line is the semiconducting fit performed in the paramagnetic phase of the barrier. This curve allows us to obtain the resistance in the absence of the magnetic
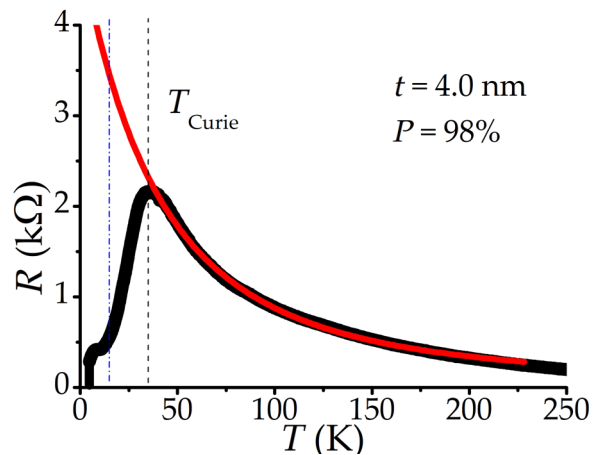

FIG. 8. Measured $R(T)$ curves (black points) and the semiconducting model fit (red straight line) above the Curie temperature T_{Curie} of the device (dashed black line) for the junction with $t = 4.0$ nm. The dash-dotted blue line indicates the temperature 15 K at which we calculate the P.

exchange field R^*. Below T_{Curie} (dashed black line), we can observe a decrease in the resistance because one spin channel is favored in the conduction.

The spin-selective tunneling processes also affect the normal resistance R_N, which is defined as $R_N = 1/(4\pi(eN(0))^2(\sigma_\uparrow + \sigma_\downarrow))$, where $N(0)$ is the density of state at the Fermi level [52].

The magnetic exchange field h in the barrier induces a magnetization in the superconducting electrodes of spin-filter JJs [52]. The angles between the magnetization in the electrodes and the magnetic exchange field will be denoted as α and β [52]. Tunneling of spin-polarized carriers appears only if the angles α and β between h and the magnetization in the left and right superconducting electrodes, respectively, are different from 0 and π [Fig. 9] [52]. The quasiparticle current in nonmagnetic devices ($P = 0, h = 0$) and in magnetic JJs with total spin polarization ($P = 1$, $h < \Delta$, where Δ is the superconducting gap of the electrodes) and maximum noncollinearity between h and the magnetization in the superconducting electrodes ($\alpha = \beta = \pi/2$) has the same analytical expression and the I-V curves are comparable [Fig. 9]. We verify this statement using the expression for the quasiparticle current in spin-filter JJs proposed in Ref. [52]. This result justifies the use of a conventional TJM model, in which there is no explicit introduction of a magnetic exchange field in the barrier, when fitting the I-V curves in the ideal case of perfect spin polarization.
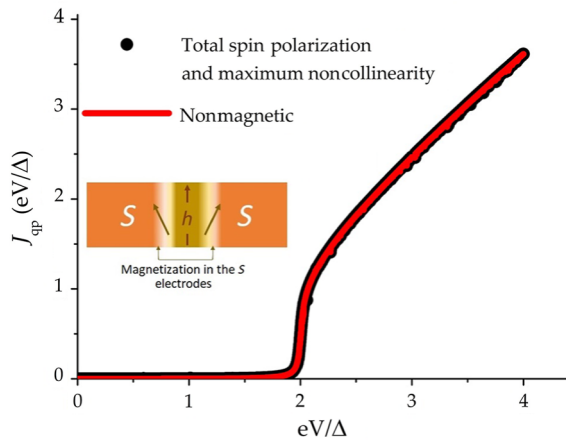

FIG. 9.   A comparison between the normalized subgap branch $J_{\text{qp}} = I_{\text{qp}}R_N/V$ for a nonmagnetic tunnel JJ (red straight line) and a perfect spin-filter tunnel JJ (black points). The expression for the quasiparticle current used for the simulations can be found in Ref. [52]. The parameters used to reproduce the curves are P = 0, $h = 0$, $\Delta = 1$, $\eta = 0.01\Delta$ (damping factor), and $T = 4.2$ K for the nonmagnetic junction and P = 1, $h = 0.4\Delta$, $\Delta = 1$, and $\eta = 0.01\Delta$ for the spin-filter JJ. The angles α and β between h and the magnetization induced in the superconducting electrodes are $\alpha = \beta = \pi/2$.

[1] F. S. Bergeret, A. F. Volkov, and K. B. Efetov, Odd triplet superconductivity and related phenomena in superconductor-ferromagnet structures, Rev. Mod. Phys. **77**, 1321 (2005).

[2] J. W. A. Robinson, J. D. S. Witt, and M. G. Blamire, Controlled injection of spin-triplet supercurrents into a strong ferromagnet, Science **329**, 59 (2010).

[3] Trupti S. Khaire, Mazin A. Khasawneh, W. P. Pratt, and Norman O. Birge, Observation of Spin-Triplet Superconductivity in Co-Based Josephson Junctions, Phys. Rev. Lett. **104**, 137002 (2010).

[4] Matthias Eschrig, Spin-polarized supercurrents for spintronics, Phys. Today **65**, 43 (2011).

[5] J. Linder and Jason W. A. Robinson, Superconducting spintronics, Nat. Phys. **11**, 307 (2015).

[6] V. V. Ryazanov, V. A. Oboznov, A. Yu. Rusanov, A. V. Veretennikov, A. A. Golubov, and J. Aarts, Coupling of Two Superconductors Through a Ferromagnet: Evidence for a π Junction, Phys. Rev. Lett. **86**, 2427 (2001).

[7] T. I. Larkin, V. V. Bol'ginov, V. S. Stolyarov, V. V. Ryazanov, I. V. Vernik, S. K. Tolpygo, and O. A. Mukhanov, Ferromagnetic Josephson switching device with high characteristic voltage, Appl. Phys. Lett. **100**, 222601 (2012).

[8] E. Goldobin, H. Sickinger, M. Weides, N. Ruppelt, H. Kohlstedt, R. Kleiner, and D. Koelle, Memory cell based on a φ Josephson junction, Appl. Phys. Lett. **102**, 242602 (2013).

[9] Bethany M. Niedzielski, T. J. Bertus, Joseph A. Glick, R. Loloee, W. P. Pratt, and Norman O. Birge, Spin-valve Josephson junctions for cryogenic memory, Phys. Rev. B **97**, 024517 (2018).

[10] A. V. Ustinov and V. K. Kaplunenko, Rapid single-flux quantum logic using π-shifters, J. Appl. Phys. **94**, 5405 (2003).

[11] A. I. Buzdin, Proximity effects in superconductor-ferromagnet heterostructures, Rev. Mod. Phys. **77**, 935 (2005).

[12] A. K. Feofanov, V. A. Oboznov, V. V. Bol'Ginov, J. Lisenfeld, S. Poletto, V. V. Ryazanov, A. N. Rossolenko, M. Khabipov, D. Balashov, A. B. Zorin, P. N. Dmitriev, V. P. Koshelets, and A. V. Ustinov, Implementation of superconductor/ferromagnet/superconductor π-shifters in superconducting digital and quantum circuits, Nat. Phys. **6**, 593 (2010).

[13] T. Kato, A. A. Golubov, and Y. Nakamura, Decoherence in a superconducting flux qubit with a π-junction, Phys. Rev. B **76**, 172502 (2007).

[14] D. Massarotti, N. Banerjee, R. Caruso, G. Rotoli, M. G. Blamire, and F. Tafuri, Electrodynamics of Josephson junctions containing strong ferromagnets, Phys. Rev. B **98**, 144516 (2018).

[15] M. Weides, M. Kemmler, E. Goldobin, D. Koelle, R. Kleiner, H. Kohlstedt, and A. Buzdin, High quality ferromagnetic 0 and π Josephson tunnel junctions, Appl. Phys. Lett. **89**, 122511 (2006).

[16] A. A. Bannykh, J. Pfeiffer, V. S. Stolyarov, I. E. Batov, V. V. Ryazanov, and M. Weides, Josephson tunnel junctions with

a strong ferromagnetic interlayer, Phys. Rev. B **79**, 054501 (2009).

[17] G. Wild, C. Probst, A. Marx, and R. Gross, Josephson coupling and Fiske dynamics in ferromagnetic tunnel junctions, Eur. Phys. J. B **78**, 509 (2010).

[18] E. Terzioglu and M. R. Beasley, Complementary Josephson junction devices and circuits: A possible new approach to superconducting electronics, IEEE Trans. Appl. Supercond. **8**, 48 (1998).

[19] L. B. Ioffe, V. B. Geshkenbein, M. V. Feigel'Man, A. L. Fauchere, and G. Blatter, Environmentally decoupled *sds*-wave Josephson junctions for quantum computing, Nature **398**, 679 (1999).

[20] S. Kawabata, S. Kashiwaya, Y. Asano, Y. Tanaka, and A. A. Golubov, Macroscopic quantum dynamics of π junctions with ferromagnetic insulators, Phys. Rev. B **74**, 180502 (2006).

[21] S. Kawabata, Y. Asano, Y. Tanaka, A. A. Golubov, and S. Kashiwaya, Josephson π State in a Ferromagnetic Insulator, Phys. Rev. Lett. **104**, 117002 (2010).

[22] A. S. Vasenko, S. Kawabata, A. A. Golubov, M. Yu. Kupriyanov, C. Lacroix, F. S. Bergeret, and F. W. J. Hekking, Current-voltage characteristics of tunnel Josephson junctions with a ferromagnetic interlayer, Phys. Rev. B **84**, 024524 (2011).

[23] R. Caruso, D. Massarotti, V. V. A. Ben-Hamida, N. L. Karelina, A. Miano, I. Vernik, F. Tafuri, V. Ryazanov, O. Mukhanov, and G. P. Pepe, RF assisted switching in magnetic Josephson junctions, J. Appl. Phys. **123**, 133901 (2018).

[24] R. Caruso, D. Massarotti, A. Miano, V. V. Bol'Ginov, A. Ben-Hamida, N. L. Karelina, G. Campagnano, I. Vernik, F. Tafuri, V. Ryazanov, O. Mukhanov, and P. G. Pepe, Properties of ferromagnetic Josephson junctions for memory applications, IEEE Trans. Appl. Supercond. **28**, 1 (2018).

[25] S. Kawabata, A. Ozaeta, A. S. Vasenko, F. W. J. Hekking, and S. F. Bergeret, Efficient electron refrigeration using superconductor/spin-filter devices, Appl. Phys. Lett. **103**, 032602 (2013).

[26] Y. Zhu, A. Pal, M. G. Blamire, and Z. H. Barber, Superconducting exchange coupling between ferromagnets, Nat. Mater. **16**, 195 (2016).

[27] J. P. Cascales, Y. Takamura, G. M. Stephen, D. Heiman, F. S. Bergeret, and J. S. Moodera, Switchable Josephson junction based on interfacial exchange field, Appl. Phys. Lett. **114**, 022601 (2019).

[28] K. Senapati, M. G. Blamire, and Z. H. Barber, Spin-filter Josephson junctions, Nat. Mater. **10**, 849 (2011).

[29] A. Pal, K. Senapati, Z. H. Barber, and M. G. Blamire, Electric-field-dependent spin polarization in GdN spin filter tunnel junctions, Adv. Mater. **25**, 5581 (2013).

[30] A. Pal, Z. H. Barber, J. W. A. Robinson, and M. G. Blamire, Pure second harmonic current-phase relation in spin-filter Josephson junctions, Nat. Commun. **5**, 3340 (2014).

[31] D. Massarotti, A. Pal, G. Rotoli, L. Longobardi, M. G. Blamire, and F. Tafuri, Macroscopic quantum tunnelling in spin filter ferromagnetic Josephson junctions, Nat. Commun. **6**, 7376 (2015).

[32] R. Caruso, D. Massarotti, G. Campagnano, A. Pal, H. G. Ahmad, P. Lucignano, M. Eschrig, M. G. Blamire, and F. Tafuri, Tuning of Magnetic Activity in Spin-Filter Josephson Junctions Towards Spin-Triplet Transport, Phys. Rev. Lett. **122**, 047002 (2019).

[33] A. Barone and G. Paterno, *Physics and Application of the Josephson Effect* (John Wiley & Sons, New York, 1982).

[34] K. K. Likharev, *Dynamics of Josephson Junctions and Circuits* (Gordon & Breach, Galsgow, 1986).

[35] D. Massarotti and F. Tafuri, in *Phase Dynamics and Macroscopic Quantum Tunneling*, edited by F. Tafuri (Springer, Cham, 2019), Vol. 286.

[36] M. H. Devoret, J. M. Martinis, D. Esteve, and J. Clarke, Resonant Activation from the Zero-Voltage State of a Current-Biased Josephson Junction, Phys. Rev. Lett. **53**, 1260 (1984).

[37] J. M. Martinis, M. H. Devoret, and J. Clarke, Experimental tests for the quantum behavior of a macroscopic degree of freedom: The phase difference across a Josephson junction, Phys. Rev. B **35**, 4682 (1987).

[38] J. M. Martinis and R. L. Kautz, Classical Phase Diffusion in Small Hysteretic Josephson Junctions, Phys. Rev. Lett. **63**, 1507 (1989).

[39] R. L. Kautz and J. M. Martinis, Noise-affected I-V curves in small hysteretic Josephson junctions, Phys. Rev. B **42**, 9903 (1990).

[40] M. H. Devoret and R. J. Schoelkopf, Superconducting circuits for quantum information: An outlook, Science **339**, 1169 (2013).

[41] P. Krantz, M. Kjaergaard, F. Yan, T. P. Orlando, S. Gustavsson, and W. D. Oliver, A quantum engineer's guide to superconducting qubits, Appl. Phys. Rev. **6**, 021318 (2019).

[42] Y. C. Chen, M. P. A. Fisher, and A. J. Leggett, The return of a hysteretic Josephson junction to the zero-voltage state: I-V characteristic and quantum retrapping, J. Appl. Phys. **64**, 3119 (1988).

[43] J. R. Kirtley, C. D. Tesche, W. J. Gallagher, A. W. Kleinsasser, R. L. Sandstrom, S. I. Raider, and M. P. A. Fisher, Measurement of the Intrinsic Subgap Dissipation in Josephson Junctions, Phys. Rev. Lett. **61**, 2372 (1988).

[44] R. Cristiano, L. Frunzio, C. Nappi, M. G. Castellano, G. Torrioli, and C. Cosmelli, The effective dissipation in Nb/AlOx/Nb Josephson tunnel junctions by return current measurements, J. Appl. Phys. **81**, 7418 (1997).

[45] V. K. Semenov, A. A. Odintsov, and A. B. Zorin, *SQUID'85—Superconducting Quantum Interference Devices and Their Applications* (Walter de Gruyter & Co., Berlin, 1985).

[46] A. Odintsov, V. Semenov, and A. Zorin, Specific problems of numerical analysis of the Josephson junction circuits, IEEE Trans. Magn. **23**, 763 (1987).

[47] S. V. Polonsky, V. K. Semenov, and P. N. Schevchenko, PSCAN: Personal superconductor circuit analyser, Supercond. Sci. Technol. **4**, 667 (1991).

[48] P. N. Schevchenko, PSCAN2: Personal superconductor circuit simulator 2 (2016), http://www.pscan2sim.org/documentation.html.

[49] D. Massarotti, D. Stornaiuolo, P. Lucignano, L. Galletti, D. Born, G. Rotoli, F. Lombardi, L. Longobardi, A. Tagliacozzo, and F. Tafuri, Breakdown of the escape dynamics in Josephson junctions, Phys. Rev. B **92**, 054501 (2015).

[50] M. G. Blamire, A. Pal, Z. H. Barber, and K. Senapati, Spin filter superconducting tunnel junctions (SPIE, 2012), Vol. 8461.

[51] PSCAN2 software (http://www.pscan2sim.org/).

[52] F. S. Bergeret, A. Verso, and A. F. Volkov, Spin-polarized Josephson and quasiparticle currents in superconducting spin-filter tunnel junctions, Phys. Rev. B **86**, 060506 (2012).

[53] J. G. Simmons, Electric tunnel effect between dissimilar electrodes separated by a thin insulating film, J. Appl. Phys. **34**, 2581 (1963).

[54] D. Massarotti, L. Longobardi, L. Galletti, D. Stornaiuolo, D. Montemurro, G. Pepe, G. Rotoli, A. Barone, and F. Tafuri, Escape dynamics in moderately damped Josephson junctions (review article), Low Temp. Phys. **38**, 263 (2012).

[55] D. Stornaiuolo, G. Rotoli, D. Massarotti, F. Carillo, L. Longobardi, F. Beltram, and F. Tafuri, Resolving the effects of frequency-dependent damping and quantum phase diffusion in YBCO Josephson junctions, Phys. Rev. B **87**, 134517 (2013).

[56] C. Bonnelle and N. Spectorv, *Rare-Earths and Actinides in High Energy Spectroscopy* (Springer International Publishing AG. Part of Springer Nature, Dordrecht, 2015), p. 109

[57] A. Kawakami, Y. Uzawa, and Z. Wang, Development of epitaxial NbN/MgO/NbN–superconductor-insulator-super

conductor mixers for operations over the Nb gap frequency, Appl. Phys. Lett. **83**, 3954 (2003).

[58] L. N. Bulaevskii, V. V. Kuzii, and A. A. Sobyanin, Superconducting system with weak coupling to the current in the ground state, JETP Lett. (USSR) (Engl. Transl.); (United States) 25, 290 (1977).

[59] M. G. Castellano, L. Grönberg, P. Carelli, F. Chiarello, C. Cosmelli, R. Leoni, S. Poletto, G. Torrioli, J. Hassel, and P. Helistö, Characterization of a fabrication process for the integration of superconducting qubits and rapid-single-flux-quantum circuits, Supercond. Sci. Technol. **19**, 860 (2006).

[60] A. V. Shcherbakova, K. G. Fedorov, K. V. Shulga, V. V. Ryazanov, V. V. Bol'Ginov, V. A. Oboznov, S. V. Egorov, V. O. Shkolnikov, M. J. Wolf, D. Beckmann, and A. V. Ustinov, Fabrication and measurements of hybrid Nb/Al Josephson junctions and flux qubits with π-shifters, Supercond. Sci. Technol. **28**, 025009 (2015).

[61] K. Serniak, M. Hays, G. de Lange, S. Diamond, S. Shankar, L. D. Burkhart, L. Frunzio, M. Houzet, and M. H. Devoret, Hot Nonequilibrium Quasiparticles in Transmon Qubits, Phys. Rev. Lett. **121**, 157701 (2018).

[62] J. Koch, Terri M. Yu, Jay Gambetta, A. A. Houck, D. I. Schuster, J. Majer, A. Blais, M. H. Devoret, S. M. Girvin, and R. J. Schoelkopf, Charge-insensitive qubit design derived from the Cooper pair box, Phys. Rev. A **76**, 042319 (2007).